Journal of Renewable and Sustainable Energy

RESEARCH ARTICLE | MARCH 23 2026

Accelerating perovskite nucleation in vacuum quenching via additive engineering for scalable inverted perovskite solar cells in ambient air

Shuxian Du; Hanxi Ge; Wenyuan Xiao; Tianyi Shao; Changxu Sun; Hao Huang ; Peng Cui ; Meicheng Li

J. Renewable Sustainable Energy 18, 023704 (2026)
https://doi.org/10.1063/5.0306380

Journal of Renewable and Sustainable Energy ARTICLE pubs.aip.org/aip/rse

Accelerating perovskite nucleation in vacuum quenching via additive engineering for scalable inverted perovskite solar cells in ambient air

Cite as: J. Renewable Sustainable Energy **18**, 023704 (2026); doi: 10.1063/5.0306380
Submitted: 10 October 2025 · Accepted: 11 March 2026 ·
Published Online: 23 March 2026

Shuxian Du, Hanxi Ge, Wenyuan Xiao, Tianyi Shao, Changxu Sun, Hao Huang,[a] Peng Cui, and Meicheng Li

AFFILIATIONS

State Key Laboratory of Alternate Electrical Power System with Renewable Energy Sources, School of New Energy, North China Electric Power University, Beijing 102206, China

[a]Author to whom correspondence should be addressed: hhuang@ncepu.edu.cn

ABSTRACT

Fabricating efficient perovskite modules is one of the prerequisites for perovskite industrialization, in which vacuum quenching is a necessary technology to regulate perovskite nucleation. In this work, we proposed an additive strategy by incorporating propylammonium chloride (PACl) into the perovskite precursor, achieving a high-quality perovskite film in ambient air. PACl is demonstrated to feasibly promote perovskite nucleation even without vacuum quenching in a wet film after coating. This effect of nucleation acceleration can also be synergistic with the vacuum quenching process, which optimizes the perovskite crystallization and reduces the residual PbI_2 located at the buried interface. Owing to the optimized perovskite film with reduced defects, the small-area inverted perovskite solar cells achieved a power conversion efficiency (PCE) of 24.59%. The device also shows excellent stability with no performance decay after 2000 h of storage in air conditions. Moreover, the large-area perovskite module with an aperture area of 47.94 cm^2 obtained a PCE of 20.24%, demonstrating the significance of our strategy for perovskite photovoltaic scalability.

INTRODUCTION

Metal halide perovskite solar cells (PSCs) have experienced rapid development due to their high power conversion efficiency (PCE), low cost, and wide range of application scenarios.[1–4] To date, the laboratory efficiency of PSCs has reached an impressive power conversion efficiency of more than 27%, comparable to that of mature silicon solar cells. In addition, the all-perovskite tandem solar has also made significant progress by achieving a PCE of more than 30%.[5–7] However, these high-efficiency PSCs are mainly based on small-area devices with an active area normally less than 1 cm^2, and the large-area perovskite modules show an obvious efficiency gap compared to these small-area PSCs.[8,9] One of the prerequisites for the perovskite industrialization is scaling up the device while maintaining as soon as possible high efficiency, in which the large-area perovskite film deposition is the key technology. Hence, it is highly desirable to understand the perovskite crystallization mechanism and propose a feasible crystallization regulation strategy to deposit high-quality, scalable perovskite film.

The vacuum quenching possesses advantages such as lower time sensitivity, higher reproducibility, and better adaptability to substrates of various sizes compared to the anti-solvent method, which has been widely adopted to deposit large-area perovskite films.[10–12] During the vacuum quenching process, most of the excess solvent is rapidly removed under high vacuum conditions, which causes the precursor concentration in the wet film to reach a critical point, leading to the instantaneous formation of numerous dense nuclei.[13,14] Numerous studies have shown that the kinetic mechanism involving rapid nucleation and subsequent slow growth facilitates the acquisition of high-crystallinity perovskite films, indicating the significance of nucleation regulation.[15,16] To demodulate the perovskite nucleation, various studies have been carried out. For example, Gao *et al.* designed a dual-pump system for accelerated vacuum depressurization alongside solvent system optimization, with the goal of modulating nucleation kinetics to achieve high-quality perovskite films.[17] Xu *et al.* employed N-ethyl-2-pyrrolidone (NEP) to modulate the nucleation process of perovskite films, which increased the nucleation sites of the α-phase during the vacuum quenching.[18] Bi *et al.* studied temperature-controlled vacuum quenching and modulated perovskite nucleation by lowering the temperature, obtaining a broader post-processing window for high-quality large-area perovskite films.[19] Although vacuum quenching can promote solvent evaporation, inducing perovskite

crystallization, the nucleation kinetics are complexly influenced by the concentration and composition of the precursor solution, the vacuum level in the chamber, as well as the ambient temperature and humidity.[20] In addition, considering that the large-area perovskite film is normally deposited in ambient air, and the moisture inevitably influences the perovskite crystallization, it is still necessary to propose a strategy to regulate the perovskite nucleation in the vacuum quenching, achieving high-quality, scalable perovskite film in ambient air.

In this work, we innovatively propose combining propylammonium chloride (PACl), a volatile additive, with vacuum flash evaporation technology to synergistically regulate the perovskite nucleation process while ensuring that no additive residue remains after crystallization optimization, thereby guaranteeing the compositional stability of the perovskite. After PACl combines with PbI_2 and undergoes deprotonation, the dissociated PA^0 volatilizes at 47.8 °C.[23,24] The measurements of scanning electron microscope (SEM), *in situ* photoluminescence (PL) (*in situ*-PL) demonstrated that PACl can be well synergistic with vacuum quenching, accelerating perovskite nucleation. This optimized nucleation kinetics further modifies the perovskite crystallization, delivering a high-quality perovskite film with reduced defect density. As a result, the inverted PSCs fabricated in ambient air obtained a PCE of 24.59%, much higher than that (23.01%) of the control PSCs. The PSCs also show excellent stability with no performance decay after 2000 h of storage in air conditions. Moreover, we also fabricated a perovskite module with an aperture area of 47.94 cm^2, achieving an efficiency of 20.24%, which demonstrates the feasibility and significance of our strategy for promoting PSC industrialization.

EXPERIMENTAL DETAILS

Experimental section

Materials

The patterned FTO (fluorine-doped tin oxide, 7 Ω sq^{-1}) glass was purchased from Advanced Electron Technology Co., Ltd. Nanoparticle powders of NiO_x (with a particle size of approximately 10 nm) and (4–(3,6-diphenyl-9H-carbazol-9-yl) butyl)phosphonic acid (Ph-4PACz) were acquired from Shanghai Weizhu Chemical Technology Co., LTD. Lead iodide (PbI_2) was procured from Tokyo Chemical Industry. C60 and bathocuproine (BCP), CsI, methylammonium chloride (MACl), methylammonium iodide (MAI), and formamidinium iodide (FAI) were obtained from Xi'an Yuri Solar Co., Ltd. N, N-dimethylformamide (DMF), N-methylpyrrolidone (NMP), propylammonium chloride (PACl), and isopropanol (IPA) were secured from Sigma-Aldrich. All chemicals were utilized directly, with no further purification.

PSCs fabrication

Patterned FTO glass substrates (1.2 × 1.8 cm^2) were sequentially ultrasonicated for 15 min in each of the following media: detergent solution, de-ionized water, ethanol, and de-ionized water. A final 40-min plasma treatment was then applied to complete the preparation process. The perovskite solar cells were fabricated under ambient conditions at 20 °C and 30%–40% RH.

NiO_x nanoparticles dispersed in water (2 mg/ml) were spin-coated (4000 rpm, 30 s) and annealed (100 °C, 10 min). Then, a Ph-4PACz solution (0.35 mg/ml) was deposited in sequence onto the NiO_x layer under the same spin-coating and annealing conditions, respectively.

The $Cs_{0.1}FA_{0.9}PbI_3$ perovskite precursor (1.5 M), with or without 8 mg of PACl, was spin-coated at 4000 rpm for 8 s. The wet film was transferred to a vacuum chamber, where the pressure dropped below 10 Pa within 7 s, followed by annealing at 100 °C for 20 mins. After cooling, the film was passivated by spin-coating a PDADI solution (1 mg/ml in IPA) and annealing at 100 °C for 10 min. Finally, the C60 (20 nm), BCP (6 nm), and Cu (100 nm) layers were sequentially deposited by thermal evaporation.

PSMs fabrication

The perovskite modules were fabricated under ambient conditions at 20 °C and 30%–40% RH. Patterned FTO glass substrates (10 × 10 cm^2) were cleaned using the same procedures as described earlier. The NiO_x precursor was prepared by dispersing NiO_x nanoparticle powder in de-ionized water (0.1 mg/ml) and spray-coated onto the heated substrates at 300 °C for rapid drying. After cooling, a Ph-4PACz layer (0.5 mg/ml in IPA) was blade-coated onto NiO_x (gap: 100 μm; speed: 16 mm/s) and annealed at 100 °C for 10 min. Subsequently, a 1.0 M $Cs_{0.05}FA_{0.85}MA_{0.1}PbI_3$ perovskite precursor (DMF: NMP, 9:1, v/v), with or without 5 mg of PACl, was blade-coated (gap: 300 μm; speed: 24 mm/s). The resulting transparent yellow wet film was transferred to a vacuum chamber to remove excess solvent, followed by annealing at 120 °C for 20 min. Finally, MeO-PEAI (0.5 mg/ml in IPA) was blade-coated (gap: 100 μm; speed: 16 mm/s) and annealed (100 °C, 10 min), before sequential thermal evaporation of C60 (20 nm), BCP (6 nm), and Cu (100 nm).

The series connection of the 10-sub-cell PSMs was defined by three laser scribes (P1, P2, P3). These were performed before substrate cleaning, before electrode evaporation, and after electrode evaporation, respectively.

RESULT AND DISCUSSION

We utilized a coating method to deposit the perovskite film based on a procedure of spin-coating or blade-coating, vacuum quenching, and then annealing. As shown in Fig. 1, first, we designed an experiment to directly reveal the effect of PACl on accelerating the perovskite nucleation through characterizing the coated film without vacuum quenching. Despite the chaotic nucleation and crystal growth caused by the absence of vacuum or anti-solvent extraction, which led to an inferior and non-uniform film, PACl still contributed to a marked improvement in the final film quality, as evidenced by its enhanced substrate coverage and reduction of PbI_2 (supplementary material, Fig. 1). However, although the PACl can optimize the perovskite formation, the final film shows an inferior crystallinity, which can be evidenced by the grew-white color. We further adopted the technology of vacuum quenching to induce perovskite nucleation. As show in Fig. 2 of the supplementary material, the wet film changed from the initial transparent light yellow to brown after vacuum quenching. As for the final perovskite film, they exhibited good crystalline quality both with and without PACl, which demonstrates the necessity of vacuum quenching in fabricating high-quality perovskite films. Based on the vacuum quenching process, we further explore the influence of PACl on the nucleation kinetics in vacuum quenching and the properties of the perovskite film.

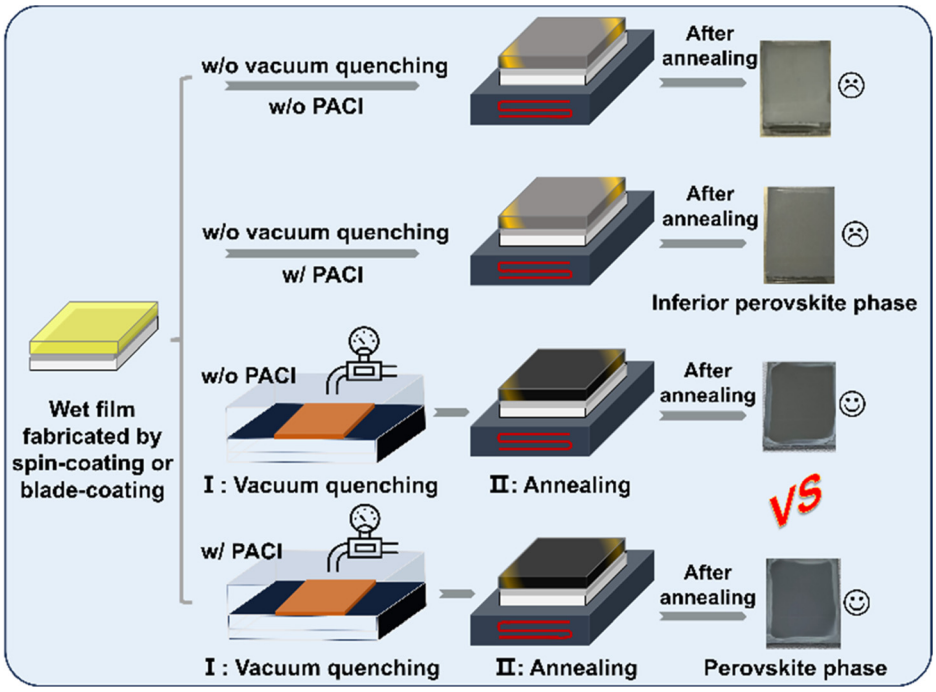

FIG. 1. Fabrication schematic of perovskite films with and without vacuum quenching and PACl.

We prepared the perovskite precursor solution and dissolved PACl into it, then characterized the FTIR spectra. The C = O peak of the solvent shifted from 1650 to 1647 cm^{-1} (supplementary material, Fig. 3), demonstrating the interaction between PACl and the perovskite precursors.[21,22] To further explore the role of PACl in regulating the crystalline quality of perovskite films alongside the vacuum quenching process, we designed a novel *in situ* photoluminescence (PL) (*in situ*-PL) characterization by combining the measurement of PL and vacuum quenching equipment to monitor the process of nucleation and pre-crystallization during solvent removal. Figures 2(a) and 2(b) show *in situ*-PL spectra of the films with and without PACl during vacuum quenching, respectively. For clarity, the sample without PACl is denoted as control, and the sample with PACl is denoted as target. During vacuum quenching, excess solvent is quickly removed under high vacuum conditions in the vacuum chamber, and the intensity of PL quickly rises. As shown in Fig. 2(c), the PL signal of the control film shows abrupt intensification at 6 s, which is earlier than the 7 s required for the target film. More importantly, the final PL intensity of the target film at the end of the vacuum quenching was much higher than that of the control film, suggesting that PACl facilitates rapid nucleation in a short period, thereby favoring the formation of a high nucleus density and the attainment of a high-quality, dense film with large grains. Vacuum quenching and PACl act synergistically to induce rapid nucleation and pre-crystallization in the target film.

To investigate the impact of PACl on the quality of perovskite films, we transferred the films after vacuum quenching to a hot plate and annealed them at 100 °C for 20 mins in ambient air. The perovskite films were deposited on the substrate of FTO/NiO_x/Ph-4PACz. The surface morphology of perovskite films was characterized by SEM,

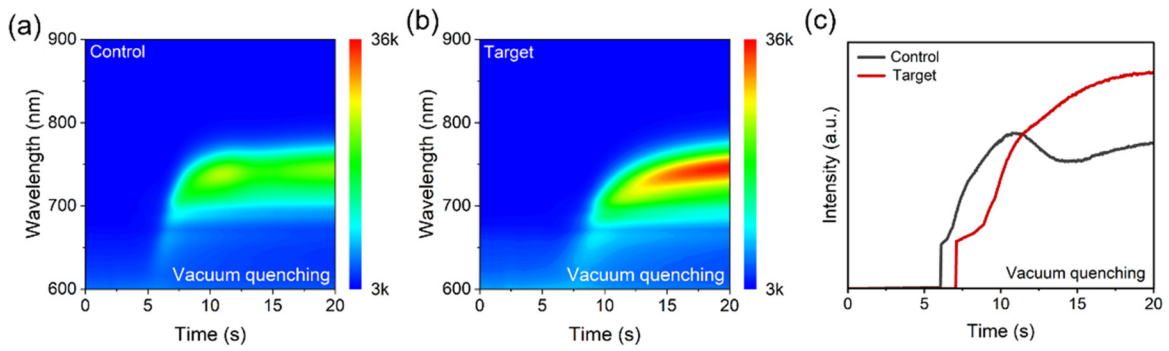

FIG. 2. (a) and (b) *In situ*-PL characterization of control and target film during vacuum quenching. (c) Maximum PL intensity as a function of vacuum quenching time, extracted from (a) and (b).

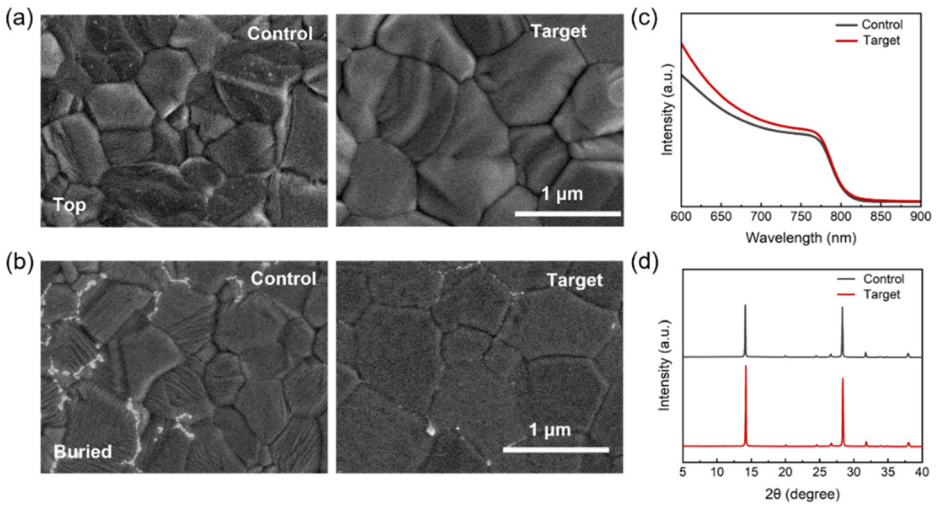

FIG. 3. (a) and (b) SEM images of annealed control and target films: (a) top surface, (b) buried interface, (c) UV-vis spectra, and (d) XRD spectra of control and target films.

which shows that the grain size of the target perovskite film increases significantly [Fig. 3(a)]. The nucleation of perovskite occurs mainly at the solution/air interface, because the solution evaporates first from the top, so the perovskite crystallizes. In the vacuum quenching process, the upper solution is extracted first, which may cause an insufficient reaction at the bottom interface, leaving residual PbI_2. We peeled off the perovskite film to reveal and observe the morphology of the buried interface. The PbI_2 phase in the control film stems from incomplete transformation to perovskite, while it is almost absent in the target film, indicating that PACl promotes uniform and dense nucleation [Fig. 3(b)]. We hypothesize that PACl may make the crystallization process more controllable and more ordered.

We further investigated the photoelectronic properties of the control and target perovskite films and their corresponding devices. As shown in Fig. 3(c), UV-vis spectra show that target perovskite films demonstrate stronger light absorption ability, which may translate into an improved current density for PSCs. To investigate the influence of PACl on the crystallization of the perovskite phase, we performed x-ray diffraction (XRD). Both the control and target perovskite films exhibited identical diffraction peaks at around 14°and 28°, corresponding to the (100) and (200) crystal planes of the perovskite phase, respectively. The virtual absence of other diffraction peaks suggests high phase purity. The significantly higher intensity of the (100) and (200) diffraction peaks in the target film indicates that PACl molecules promote the growth of characteristic crystal planes and enhance the overall crystallinity [Fig. 3(d)].

The improved crystallinity of the perovskite film is beneficial for reducing defect density. We fabricated the control and target perovskite films on glass substrates and then carried out PL, time-resolved PL (TRPL), and space-charge limited current (SCLC) measurements to characterize the non-radiative defects. As shown in Fig. 4(a), the PL intensity of the target perovskite film is stronger than that of the control perovskite film. The fitted TRPL results [Fig. 4(b)] show that the target perovskite film has a longer carrier lifetime, prolonging from 2.02 to 2.69 μs compared to the control perovskite film. Furthermore, we fabricated electron-only and hole-only devices to carry out the SCLC measurements. The trap filling limit voltage (V_{TFL}) in electron-only devices of the control and target are 0.79 and 0.34 V, respectively. The trap density (N_{trap}) decreases from 26.98×10^{15} to $11.27 \times 10^{15}\,cm^{-3}$, calculated according to the equation of $N_{trap} = 2\varepsilon_r\varepsilon_0 V_{TFL}/eL2$ (ε_r is the relative permittivity, ε_0 is the vacuum permittivity, e is the electron charge, L is the perovskite film thickness, and V_{TFL} is the limiting voltage full of traps). The V_{TFL} in hole-only devices of control and target films are 0.24 and 0.19 V, respectively.

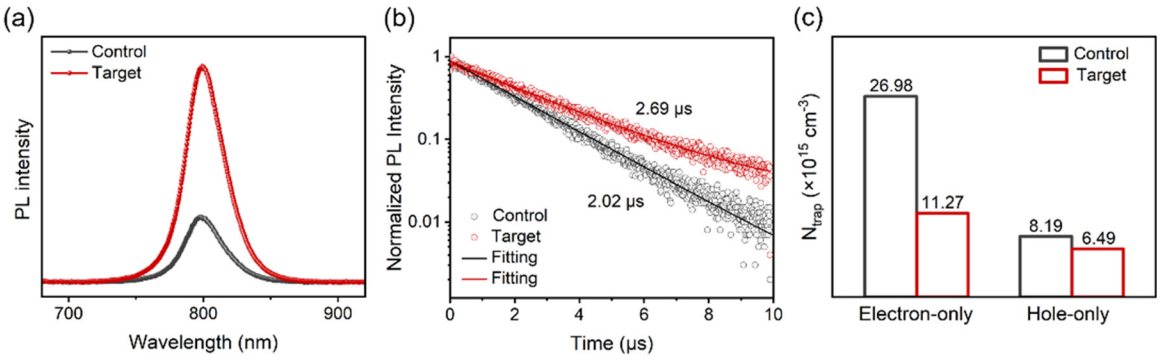

FIG. 4. (a) PL spectra and (b) TRPL fitting results of control and target films. (c) SCLC curves for electron-only and hole-only devices.

The N_{trap} decreases from 8.19×10^{15} to 6.49×10^{15} cm^{-3} [Fig. 4(c), supplementary material, Fig. 4]. These results show that the perovskite films with PACl-assisted crystallization exhibit better crystal quality and fewer defects.

The vacuum quenching technique, combined with the PACl additive, promoted nucleation and pre-crystallization, resulting in a smooth, compact perovskite film with low defect density, which is a prerequisite for improving the performance of PSCs. We characterized the photovoltaic parameters, including power conversion efficiency (PCE), short circuit current density (J_{SC}), open circuit voltage (V_{OC}), and fill factor (FF), to assess the performance improvement. After determining the optimal concentration of PACl, we systematically investigated the performance enhancement enabled by this method (supplementary material, Fig. 5). As shown in Fig. 5(a), the target PSCs achieve the champion PCE of 24.59%, with a J_{SC} of 25.65 mA cm^{-2}, a V_{OC} of 1.147 V, and an FF of 83.52%. In contrast, the control PSCs only achieve a champion PCE of 23.01%, with a J_{SC} of 25.47 mA cm^{-2}, a V_{OC} of 1.121 V, and an FF of 80.57%. Meanwhile, the forward PCE of control and target PSCs is shown in Fig. 6 of the supplementary material, which shows a negligible hysteresis in target devices. The external quantum efficiency (EQE) confirms that the J_{SC} of PSCs is reliable (supplementary material, Fig. 7). Figure 5(b) shows the PCE distribution histograms of 40 control and target PSCs, respectively. The results demonstrate a narrow distribution for target PSCs, indicating good reproducibility and a higher average PCE of 24.06% compared to the PCE of 21.97% for the control PSCs. The corresponding statistics of J_{SC}, V_{OC}, and FF are presented in supplementary material, Fig. 8. Furthermore, the stability of control and target PSCs was studied by measuring the steady-state power output for 300 s in ambient air. As shown in Fig. 5(c), the target PSCs possess a PCE of 24.20% with negligible decay after tracking for 300 s under a bias voltage of 0.989 V, while the PCE of control PSCs decays from 22.79% to 22.54% under a bias voltage of 0.950 V. The results indicate that the enhanced stability of target PSCs results from the accelerated nucleation during vacuum quenching and enables the formation of a superior pre-crystallized film. Unencapsulated control and target PSCs were stored in an environment with 25% RH and 25 °C. Five samples were tested in each group to ensure data reliability. The results show that the target PSCs retained nearly 100% of their initial PCE after 2000 h, demonstrating a significant enhancement in operational stability [Fig. 5(d)]. Both the steady-state power output and storage stability tests confirmed the enhanced stability of the target PSCs. Building on these findings, we further investigated the operational stability of unencapsulated target PSCs under continuous illumination in a N_2 glovebox, maintaining a device temperature of approximately 50 °C throughout the testing. After more than 250 h of continuous testing, the target PSCs retained 97% of its initial PCE [Fig. 5(e)]. We placed the unencapsulated PSCs in a dark environment at 85 °C, and after 100 h, the target device retained 97% of their initial PCE (23.72%), while the control sample decreased to 83% of its initial value (22.83%) (supplementary material, Fig. 9). These results demonstrate that promoting nucleation and pre-crystallization enables highly efficient and stable perovskite solar cells.

Scaling up the area of efficient perovskite solar cells is a prerequisite for industrialization. Therefore, we investigated the fabrication processes for PSMs using vacuum quenching technology. As shown in Fig. 6(a), the target PSMs achieve a champion PCE of 20.24% ($J_{SC} = 2.32$ mA cm^{-2}, $V_{OC} = 10.96$ V, and FF = 79.48%), while the control PSMs achieve a champion PCE of 19.62% ($J_{SC} = 2.29$ mA cm^{-2}, $V_{OC} = 10.88$ V, and FF = 79.48%). The improved performance of the target PSMs stems from the enhanced crystallinity of the perovskite film, combined with a lower defect density. Then, we connected the PSMs to a fan and placed it outdoors under sunlight. The successful operation of the fan confirmed the practical functionality of perovskite modules [Fig. 6(b)].

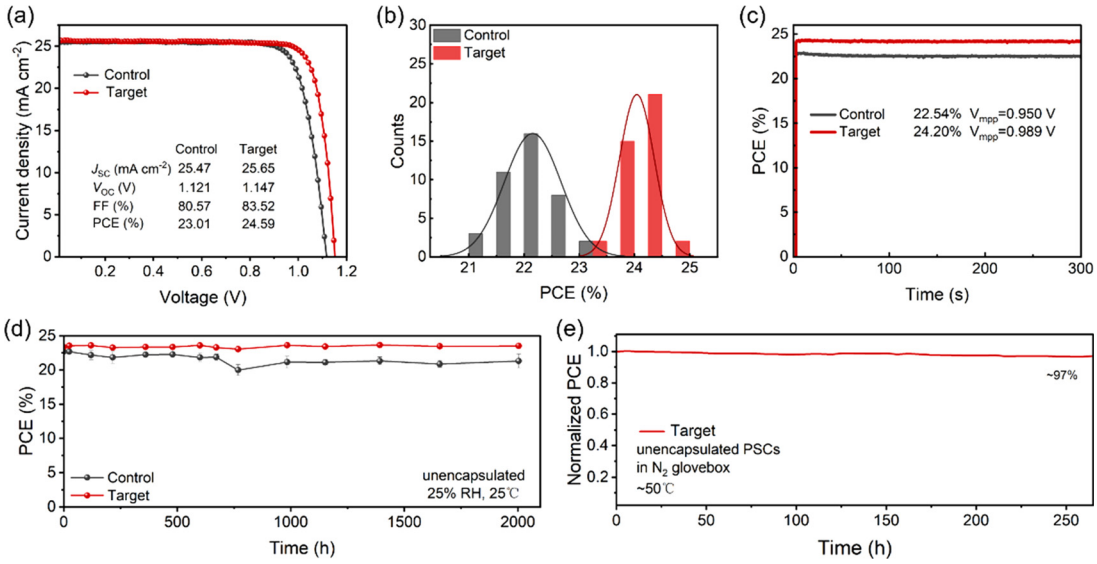

FIG. 5. (a) PCE of control and target PSCs. (b) Distribution of PCE. (c) Steady-state power output for 300 s. (d) PCE evolution of unencapsulated PSCs stored under ambient air at 25% RH and 25 °C. (e) Operational stability of the unencapsulated PSCs under continuous 1-sun illumination in N_2 glovebox.

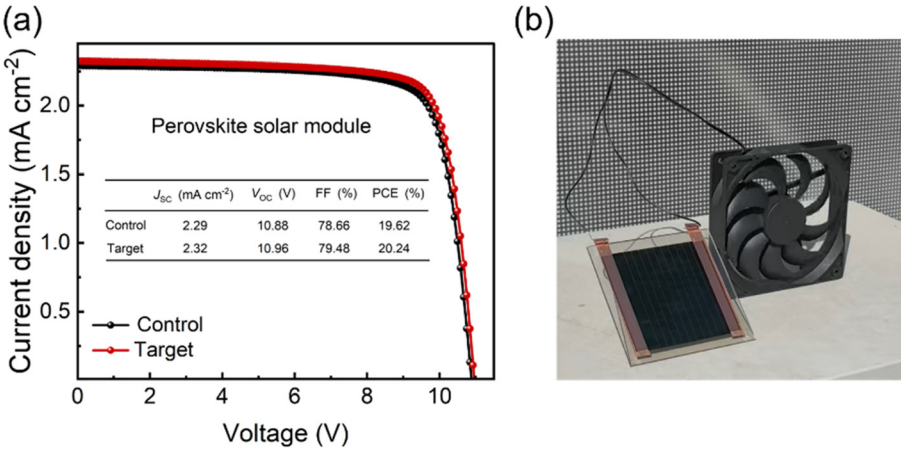

FIG. 6. (a) PCE of control and target PSMs. (b) The PSMs power the fan.

CONCLUSION

In summary, we proposed an additive strategy by incorporating PACl into the perovskite precursor to modulate the perovskite nucleation in vacuum quenching, which contributes to obvious performance enhancement in the ambient-air-processed PSCs. The *in situ*-PL demonstrated that PACl can effectively accelerate the perovskite nucleation in the vacuum quenching process, optimizing the perovskite crystallization with a larger grain size. In addition, the PACl can also reduce the residual PbI2 located at the buried interface. Owing to the reduced defect density in the perovskite film, the resulting PSCs with PACl achieved a PCE of 24.65%, which is higher than that (23.01%) of control PSCs. The device can maintain nearly 100% of its initial PCE after 2000 h of aging in an ambient condition, demonstrating a satisfying storage stability. In addition, the large-area perovskite module achieved a PCE of 20.24%, indicating the feasibility of our strategy for scalable devices. Our work proposed a nucleation acceleration strategy and revealed the critical influence of nucleation kinetics in vacuum quenching on the film property and device performance, providing more opportunities to fabricate high-performance, scalable perovskite photovoltaics.

SUPPLEMENTARY MATERIAL

See the supplementary material for additional materials, including SEM images of perovskite films with and without PACl, prepared without vacuum quenching; pictures of wet perovskite films before and after vacuum quenching; FTIR spectra of perovskite precursor with and without PACl; dark current–voltage characteristics of control and target devices; optimum *J*–*V* curves of the small-area devices with different PACl modification concentrations; *J*–*V* curves (forward scan) of control and target PSCs; EQE of target PSCs; (a) J_{SC}, (b) V_{OC}, (c) FF of control and target PSCs; and the stability of unencapsulated perovskite solar cells at 85 °C in the dark.

ACKNOWLEDGMENTS

This work was partially supported by the National Natural Science Foundation of China (Grant Nos. 52402254, 52232008, 52102245, and 22409061), the Beijing Natural Science Foundation (Z240024), the Beijing Nova Program (No. 20220484016), the Young Elite Scientists Sponsorship Program by CAST (No. 2022QNRC001), the Huaneng Group Headquarters Science and Technology Project (No. HNKJ20-H88), the Fundamental Research Funds for the Central Universities (Nos. 2023MS042, 2024MS036, 2023MS047, 2024MS039, and 2024JC005), and the NCEPU "Double First-Class" Program.

AUTHOR DECLARATIONS

Conflict of Interest

The authors have no conflicts to disclose.

Author Contributions

Shuxian Du: Conceptualization (equal); Data curation (equal); Formal analysis (equal); Investigation (equal); Methodology (equal); Writing – original draft (equal); Writing – review & editing (equal). **Hanxi Ge:** Data curation (equal); Formal analysis (equal); Methodology (equal); Visualization (equal). **Wenyuan Xiao:** Data curation (equal); Formal analysis (equal); Writing – original draft (equal). **Tianyi Shao:** Data curation (equal); Formal analysis (equal); Methodology (equal). **Changxu Sun:** Data curation (equal); Methodology (equal); Writing – original draft (equal). **Hao Huang:** Conceptualization (equal); Funding acquisition (equal); Project administration (equal); Supervision (equal); Validation (equal); Writing – review & editing (equal). **Peng Cui:** Funding acquisition (equal); Project administration (equal); Supervision (equal); Writing – review & editing (equal). **Meicheng Li:** Conceptualization (equal); Project administration (equal); Resources (equal); Supervision (equal); Writing – review & editing (equal).

DATA AVAILABILITY

The data that support the findings of this study are available from the corresponding author upon reasonable request.

REFERENCES

[1]S. Du, H. Huang, Z. Lan, P. Cui, L. Li, M. Wang, S. Qu, L. Yan, C. Sun, Y. Yang, X. Wang, and M. Li, Nat. Commun. **15**, 5223 (2024).
[2]J. Zhou, L. Tan, Y. Liu, H. Li, X. Liu, M. Li, S. Wang, Y. Zhang, C. Jiang, R. Hua, W. Tress, S. Meloni, and C. Yi, Joule **8**, 1691–1706 (2024).
[3]Y. Pan, J. Wang, Z. Sun, J. Zhang, Z. Zhou, C. Shi, S. Liu, F. Ren, R. Chen, Y. Cai, H. Sun, B. Liu, Z. Zhang, Z. Zhao, Z. Cai, X. Qin, Z. Zhao, Y. Ji, N. Li, W. Huang, Z. Liu, and W. Chen, Nat. Commun. **15**, 7335 (2024).

[4]H. Meng, K. Mao, F. Cai, K. Zhang, S. Yuan, T. Li, F. Cao, Z. Su, Z. Zhu, X. Feng, W. Peng, J. Xu, Y. Gao, W. Chen, C. Xiao, X. Wu, M. D. McGehee, and J. Xu, Nat. Energy **9**, 536–547 (2024).
[5]NREL, see www.nrel.gov/pv/cell-eficiency. Html for "National renewable energy laboratory best research cell efficiency chart" (NREL, 2024).
[6]M. A. Green, E. D. Dunlop, M. Yoshita, N. Kopidakis, K. Bothe, G. Siefer, X. Hao, and J. Y. Jiang, Prog. Photovoltaics Res. Appl. **33**, 795–810 (2025).
[7]H. Guan, S. Fu, W. Chen, W. Ke, G. Fang, and W. Feng, DeCarbon **8**, 100098 (2025).
[8]S. Liu, J. Li, W. Xiao, R. Chen, Z. Sun, Y. Zhang, X. Lei, S. Hu, M. Kober-Czerny, J. Wang, F. Ren, Q. Zhou, H. Raza, Y. Gao, Y. Ji, S. Li, H. Li, L. Qiu, W. Huang, Y. Zhao, B. Xu, Z. Liu, H. J. Snaith, N.-G. Park, and W. Chen, Nature **632**, 536–542 (2024).
[9]Y. Wang, R. Lin, C. Liu, X. Wang, C. Chosy, Y. Haruta, A. D. Bui, M. Li, H. Sun, X. Zheng, H. Luo, P. Wu, H. Gao, W. Sun, Y. Nie, H. Zhu, K. Zhou, H. T. Nguyen, X. Luo, L. Li, C. Xiao, M. I. Saidaminov, S. D. Stranks, L. Zhang, and H. Tan, Nature **635**, 867–873 (2024).
[10]X. Li, D. Bi, C. Yi, J.-D. Décoppet, J. Luo, S. M. Zakeeruddin, A. Hagfeldt, and M. Grätzel, Science **353**, 58–62 (2016).
[11]D. Bi, X. Li, J. V. Milić, D. J. Kubicki, N. Pellet, J. Luo, T. LaGrange, P. Mettraux, L. Emsley, S. M. Zakeeruddin, and M. Grätzel, Nat. Commun. **9**, 4482 (2018).
[12]S. Yuan, D. Zheng, T. Zhang, Y. Wang, F. Qian, L. Wang, X. Li, H. Zheng, Z. Diao, P. Zhang, T. Pauporté, and S. Li, Nat. Commun. **16**, 2052 (2025).
[13]S. Ternes, F. Laufer, and U. W. Paetzold, Adv. Sci. **11**, 2308901 (2024).
[14]B. Yan, W. Dai, Z. Wang, Z. Zhong, L. Zhang, M. Yu, Q. Zhou, Q. Ma, K. Yan, L. Zhang, Y. Yang, and J. Yao, Science **388**, eadt5001 (2025).
[15]L. Zeng, S. Chen, K. Forberich, C. J. Brabec, Y. Mai, and F. Guo, Energy Environ. Sci. **13**, 4666–4690 (2020).
[16]Z. Xu, Z. Guo, H. Li, Y. Zhou, Z. Liu, K. Wang, Z. Li, H. Wang, S. Qaid, O. Mohammed, and Z. Zang, Energy Environ. Sci. **18**, 1354–1365 (2025).
[17]J. Gao, F. Fei, Y. Xu, S. Wang, Y. Li, K. Du, H. Sun, X. Dong, N. Yuan, and L. Li, ACS Appl. Mater. Interfaces **16**, 38017 (2024).
[18]Y. Xu, C. Zhou, X. Li, K. Du, Y. Li, X. Dong, N. Yuan, L. Li, and J. Ding, Small Methods **8**, 2400428 (2024).
[19]L. Bi, J. Wang, Z. Zeng, X. Ji, X. Huang, F. R. Lin, S.-W. Tsang, Q. Fu, and A. K. Y. Jen, Nat. Photonics **19**, 968–976 (2025).
[20]H. Hu, D. B. Ritzer, A. Diercks, Y. Li, R. Singh, P. Fassl, Q. Jin, F. Schackmar, U. W. Paetzold, and B. A. Nejand, Joule **7**, 1574–1592 (2023).
[21]H. Yun, H. W. Kwon, M. J. Paik, S. Hong, J. Kim, E. Noh, J. Park, Y. Lee, and S. I. Seok, Nat. Energy **7**(9), 828–834 (2022).
[22]S. Li, H. Qin, M. Zuo, W. Xu, Y. Xia, L. Chao, and Y. Chen, J. Mater. Chem. A **14**, 8595 (2026).
[23]J. Park, J. Kim, H. Yun, M. J. Paik, E. Noh, H. J. Mun, M. G. Kim, T. J. Shin, and S. I. Seok, Nature **616**, 7958, 724 (2022).
[24]Y. Zhang, Y. Li, L. Zhang, H. Hu, Z. Tang, B. Xu, and N. Park, Adv. Mater. **11**, 2102538 (2021).